Journal of Power Sources 197 (2012) 224–230

Contents lists available at SciVerse ScienceDirect

Journal of Power Sources

journal homepage: www.elsevier.com/locate/jpowsour

In situ study of topography, phase and volume changes of titanium dioxide anode in all-solid-state thin film lithium-ion battery by biased scanning probe microscopy

Jing Zhu, Jinkui Feng, Li Lu, Kaiyang Zeng*

Department of Mechanical Engineering, National University of Singapore, 9 Engineering Drive 1, 117576, Singapore

ARTICLE INFO

Article history:
Received 15 July 2011
Received in revised form 24 August 2011
Accepted 25 August 2011
Available online 7 September 2011

Keywords:
All-solid-state thin film Li-ion battery
In situ atomic force microscopy
Li-ion distribution

ABSTRACT

In this study, local cyclic changes of surface topography, phase and volume of TiO_2 anode within an all-solid-state thin film Li-ion battery (TiO_2/LiPON/$LiNi_{1/3}Co_{1/3}Mn_{1/3}O_2$) at nanoscale are studied. These changes are caused by reversible bias-induced electric field through an in situ scanning probe microscopy (SPM) without external electrochemical attachment. Combining simultaneous measurements of phase and amplitude images, high spatially resolved mapping of "nano-spots" related to Li+ distribution can be obtained, providing new insight into the ionic transport mechanism and diffusion preferred paths in a real all-solid-state thin film lithium ion battery. In addition, the thin film anode shows reversible topographical changes as the volume expansion/contraction is related to the cyclic Li+ insertion/extraction, which are analogues to the charge/discharge behavior observed in electrochemical atomic force microscopy (EC-AFM) studies. The results suggest that the applications of local reversible biases are very useful for modeling the charge/discharge processes of lithium ion batteries.

1. Introduction

Recently, rapid advances in micro- and nano-fabrication technologies have largely reduced the scale, the current density and the power requirement of electronic device to extremely lower levels, driving the development of the all-solid-state thin film Li-ion batteries which can be integrated into the electronic devices and micro-electromechanical systems (MEMS), such as integrated circuits, smart cards, implanted medical devices, and semiconductor chips [1–3]. Since all of the electrochemical processes are confined in an internal multilayer structure, all-solid-state thin film batteries are also significant tools to investigate the electrochemical mechanisms of solid electrode/electrolyte without binders and perform in situ characterizations. To optimize the energy density and life time of lithium ion batteries, numerous studies have been focused on the electrochemical mechanisms from macroscopic to microscopic levels. However, due to the limitation of experimental and analysis methods, microscopic mechanisms involving the ionic diffusion, charge and vacancy trapping, local phase transformation, and electrode/electrolyte interfacial phenomenon are still not very clear [4]. During the last two decades, scanning probe microscopy (SPM) technique has emerged as a powerful tool to characterize multiple properties of functional materials with high spatial resolution, such as topography, piezoelectricity, conductivity, charge distribution, and electrostatic surface potential of ferroelectrics and semiconductors [5–8]. Recently, several groups have applied SPM techniques to the field of energy storage system in order to study the micro and nanoscale electrochemical functionalities, such as those in lithium ion batteries [9–19]. However, previous in situ SPM studies were mainly conducted using special electrochemical atomic force microscopy (EC-AFM), such as electrochemical scanning tunneling microscopy (EC-STM), electrochemical impedance spectroscopy (EIS), as well as newly developed electrochemical strain microscopy (ESM) [4,9–11,17,18], or combining with the external electrochemical attachments including electrometer or potentioastat [19–26]. In this study, we propose a new in situ method using biased scanning probe microscopy (SPM) without other external attachment to induce Li+ diffusion within the all-solid-state thin film battery, while monitoring the cyclic changes of topography, phase and volume of thin film anode. In this work, an all-solid-state thin film Li-ion battery, which consists of TiO_2 anode, LiPON electrolyte, and $LiNi_{1/3}Co_{1/3}Mn_{1/3}O_2$ cathode, is selected as the test model. Different from the recent published ESM studies [4,9–11,17,18], the bias applied in this work is only within the range of ± 3 V, which is significant lower than that ($\sim \pm 15$ V) used in the literatures. In addition, single layer of electrode film is also studied to identify the effects of Li+ diffusion. Fig. 1(a) and (b) shows the schematic drawing of the in situ SPM experimental

* Corresponding author. Tel.: +65 6516 6627; fax: +65 6779 1459.
E-mail address: mpezk@nus.edu.sg (K. Zeng).

0378-7753/$ – see front matter © 2011 Elsevier B.V. All rights reserved.
doi:10.1016/j.jpowsour.2011.08.115

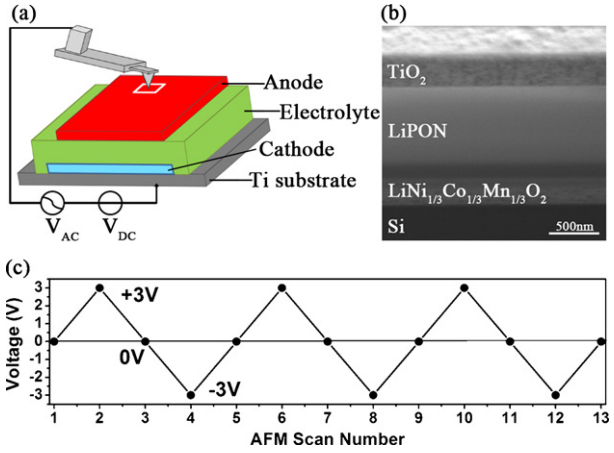

Fig. 1. (a) Schematic of the in situ SPM measurement used in this study. The active battery area is overlapping portion of the anode and cathode layer. A 1 μm × 1 μm area indicated by the white line was scanned by SPM with a conductive probe. (b) FIB cross-sectional image of the thin film battery. (c) Cyclic electrical signal applied to the battery to probe Li-ion diffusion *vs.* SPM scan number.

set-up and the cross-sectional image illustrating the layout of thin film battery (using Focused Ion Beam (FIB)), respectively. Noted that the thin film Li-ion battery used here has full electrochemical functionality (reversible charge/discharge capacity) once current collector is deposited; and the cycling performance has been studied previously. For all-solid-state thin film Li-ion batteries, most of previous studies focused on lithium metal anode [16,27]. In this study, polycrystalline TiO_2, which is a promising anode material due to its low cost and high capacity, is selected as thin film anode. Therefore, it is necessary to study its microscopic electrochemical mechanisms using in situ SPM measurement. The ideal lithium ion battery consists of cathode and anode separated by electrolyte which is a good Li+ conductor and electron insulator. Due to different electrochemical potentials of lithium in the two electrodes, the diffusion of Li+ from the cathode through the electrolyte into the anode is compensated by the transfer of the electron from the anode to the cathode through the external circuit. Therefore, we apply a series of biases through the SPM tip in contact mode (dc-writing) using electric force microscopy (EFM), followed by scanning the biased region in tapping mode. The applied cyclic biases induce reversible Li+ diffusion within the battery while the conductive tip acts as a current collector for TiO_2 anode. The schematic of waveform cyclic voltage within ±3 V and SPM scanning interval are shown in Fig. 1(c). In this study, topographical changes caused by volume expansion/contraction under cyclic electric field can reveal the bias-induced Li+ concentration changes at nanoscale. Information on the distribution of Li+ diffusion preferred paths around the surface of the thin film anode can also be provided by combining the simultaneous measurements of phase and amplitude. This in situ study gives the understanding of microscopic electrochemical mechanisms of polycrystalline TiO_2 anode in real all-solid-state thin film Li-ion battery, providing a new insight on metal oxide as anode in lithium ion batteries.

2. Experimental

2.1. Sample preparation

All-solid-state thin film Li-ion battery samples were deposited by magnetron sputtering on Si substrate for FIB cross-sectional image, and on pure Ti substrate for in situ SPM studies, respectively. The pure Ti substrate (1 cm diameter and 1 mm thick) was previously polished to a mirror-like surface. The ~0.25 μm thick $LiNi_{1/3}Co_{1/3}Mn_{1/3}O_2$ cathode film was first deposited on the substrate using rf sputtering at 100 W in Ar/O_2 (3:1) mixed gas condition. The substrate temperature was kept at 700 °C. Target for the cathode (2 in. diameter and 3 mm thick) was fabricated in-house using commercial powders, which were cold-pressed into a pellet followed by sintering in air at 900 °C for 15 h. After the deposition of cathode film, the ~1 μm thick LiPON electrolyte was deposited sequentially by rf sputtering (60 W) in N_2 atmosphere at room temperature, using a Li_3PO_4 target (Super Conductor Materials, Inc., 2 in. diameter and 3 mm thick). Finally, the ~0.25 μm thick TiO_2 thin film anode was deposited from a titanium metal under O_2 atmosphere.

2.2. In situ scanning probe microscopy

A commercial SPM system (MPF-3D, Asylum Research, USA) was used as the characterization tool in this study. As shown in Fig. 1(a), the conductive substrate was electrically connected to the SPM system. An effective battery area covering the entire cathode/electrolyte/anode structure was scanned by a Pt-coated conductive tip (Electri-Lever, Olympus, Japan, tip radius <15 nm) under the ambient condition. The resonant frequency of the tip is about 75 Hz with a spring constant of 2 N m^{-1}. EFM operated in contact mode was used to apply biases through the conductive tip (dc writing). A series of biases within ±3 V was applied (with the frequency of 1 Hz) to the anode surface in 1 μm × 1 μm area to induce the cyclic Li+ diffusion. The advantage of using symmetrical voltages is to ensure that the total amount of Li+ diffusion within the battery is reversible and constant. After the dc-writing process, in situ SPM scanning was performed in tapping mode to obtain height, deflection and phase images simultaneously. All SPM images were generated by a pixel density of 256 × 256 and a scan rate of 1 Hz. Other scanning parameters were also optimized for obtaining high-quality images.

3. Results and discussions

3.1. Surface topography

Fig. 2 shows the results of in situ SPM experiments performed on TiO_2 thin film anode within the all-solid-state thin film Li-ion battery subjected to cyclic voltages. All images are captured continuously from the same location. However, slight shift of scanning area, which is still a major technical challenge, cannot be prevented due to the continuous monitoring using SPM. Left columns in Fig. 2 are typical topography images in height mode. The as-deposited TiO_2 film consists of scale-shaped nano-grains with average grain size less than 10 nm [Fig. 2(a)]. After the first Li+ insertion cycle (applying +3 V), film surface has become flat since the grains of thin film anode grow and expand almost uniformly in all directions with the grain boundaries contacting seamlessly [Fig. 2(b)], which is induced by Li+ migrating from $LiNi_{1/3}Co_{1/3}Mn_{1/3}O_2$ cathode into TiO_2 anode under the electric field. During the first Li+ extraction cycle (applying −3 V), shrinkage of the film can be observed evidently as Li+ is removed from the anode, and the gaps between inter particles have become sharper (indicated by the black arrows in Fig. 2(b) and (c)). As Li+ is inserted into the thin film anode again during the second Li+ insertion cycle, the film expands along the original gap lines [Fig. 2(d)], and followed by an obvious contraction during the second Li+ extraction cycle [Fig. 2(e)]. Fig. 3 shows three dimensional images scanned from the same area as in Fig. 2, where the reversible morphology changes are more evident. As discussed earlier, there is an obvious topography change related to the expansion of thin film anode during the first Li+ insertion cycle, most of boundaries and gaps between the particles have

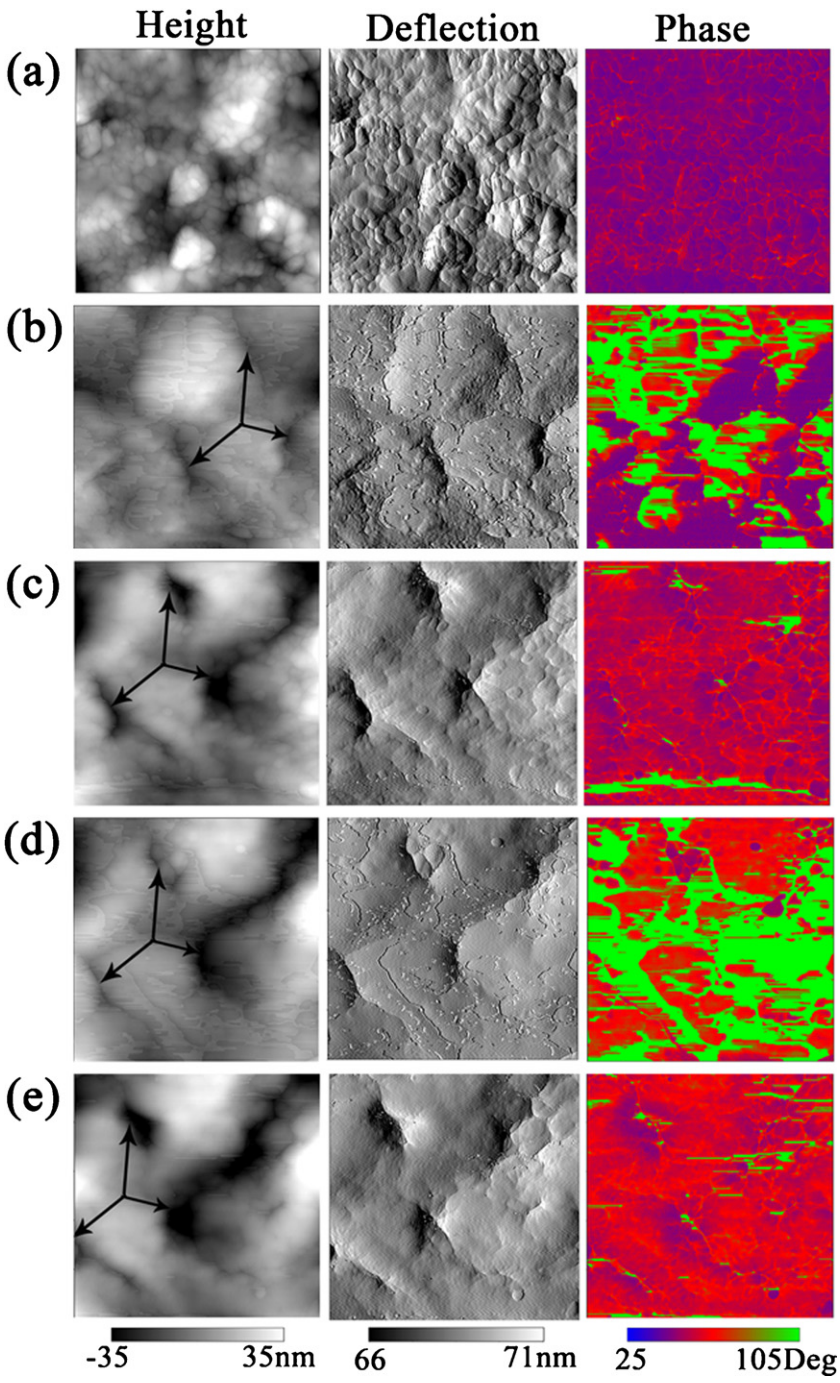

Fig. 2. In situ SPM images of thin film anode in the selected thin film Li-ion microbattery polarized to cyclic potential. From left to right column: height images, deflection images and phase images. (a) Scan 1; (b) scan 2; (c) scan 4; (d) scan 6; and (e) scan 8.

been filled up and closed, excepting a few deep gaps [Fig. 3(a) and (b)]. During the second cycle, the topographical changes are especially evident in the original particle gaps marked by the black circles in Fig. 3(b)–(d), where the gaps are closed and reopened reversibly under the reversible electric field. Subsequent Li+ insertion/extraction cycles show similar morphology changes, i.e., the expansion/shrinkage of particle gaps or boundaries, which become smaller through lithiation and deeper through delithiation. It can be proved that the reversible morphology changes are not surface damage (such as the scratch made by SPM tip), but attributed to the cyclic Li+ diffusion. This insertion/extraction behavior of Li+ is similar to the findings by Koltypin et al. on graphite anode [15]. Therefore, similar to traditional electrochemical measurements, the local cyclic biases applied through SPM tip can also induce analogous Li+ diffusion and further morphology changes. In this study, to induce Li+ transportation between anode and cathode reversibly by SPM, the amplitude of cyclic voltage (±3 V) is beyond the normal operation voltage range of a typical lithium ion battery. Thus, the same in situ measurement is also conducted on single layer $LiNi_{1/3}Co_{1/3}Mn_{1/3}O_2$ cathode to verify whether the cathode film is damaged under such voltage. The results show that neither the full battery nor cathode film shows any permanent damage, since the contact intensity and time of tip-induced bias is much lower than that used in the traditional electrochemical measurement. Since the cyclic biases are applied through the SPM tip scanning, the scanning rate should be comparable to the diffusion time of

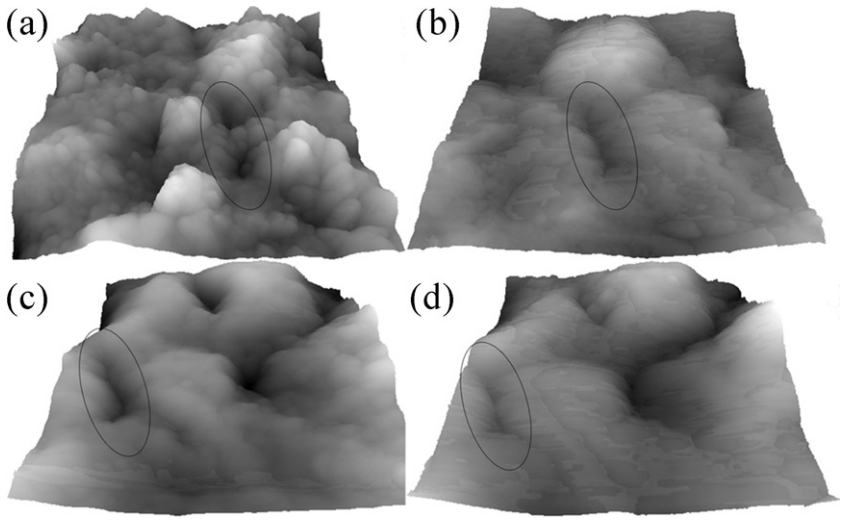

Fig. 3. In situ 3D topography images (1 μm × 1 μm) of Fig. 2 (at the same location): (a) scan 1; (b) scan 2; (c) scan 4; and (d) scan 6.

Li+. Noted that the typical Li+ diffusion rate is between 1×10^{-14} and 1×10^{-12} $m^2 s^{-1}$, the diffusion time of Li+ is about ~0.1–1 s if the tip radius is between 10 and 100 nm [11]. Considering the tip radius, dc-writing frequency of 1 Hz used in this experiment is therefore enough to induce Li+ diffusion.

3.2. Cyclic bias-induced phase transition

Generally speaking, phase images not only provide clear observation of micro and nano surface structures that are invisible or barely visible in height images, but also reflect variations in compositions and other surface properties, such as surface energy. However, the interpretation of phase image is complex and still a challenge issue, requiring fundamental understanding of the physics at atomic level. The differences in compositions and adherence properties near the sample surface result in the variations of energy dissipated through the tip-sample interactions, leading to phase angle shift due to the difference between the freely cantilever oscillating in air and the oscillation during scanning [28–30]. Therefore, the contrast in phase image is mainly due to the variations of phase angle shift. The darker regions represent smaller phase angle shift associated with higher energy dissipation, while the brighter regions represent larger phase angle shift related to lower energy dissipation. Thus, the brighter regions correspond to the harder phases with higher surface stiffness or adhesion force, which interact more strongly with the SPM tip. Fig. 2 (right column) shows phase image evolution of TiO_2 film under cyclic applied voltages. The scales are identical for all images as seen in the color bar at the bottom. As shown in Fig. 2(a), no clear contrast in phase image can be observed for as-deposited film besides the brighter lines corresponding to the grain boundaries in topography. When cyclic voltages are applied, the phase images show different features indicating the occurrence of biased-induced phase transitions. New phase indicated by the brighter color (green) appears in phase image when the battery is first polarized to 3 V, and mostly disappears when the battery is polarized to −3 V [Fig. 2(b) and (c)]. From the color contrast shown in the phase images, similar phase changes can be observed during the first two cycles, the phase shift is positive after the positive polarization but negative after the negative polarization. This result can be further supported by the phase angle analysis. The phase angle distributions during the first cycle are plotted as histograms in Fig. 4(a). The mean value is determined by fitting data using Gaussian function theory. There is only one remarkable peak for as-deposited film with the mean phase angle of about ~45°, corresponding to polycrystalline TiO_2 phase (red color bin). After the first Li+ insertion cycle (applying +3 V), the peak intensity of the main phase (green color bin) becomes lower than that of the as-deposited film; and a new phase has emerged at about ~131°, which is presumably attributed to Li+ diffusion and the related electrochemical transformation. In contrast, the peak intensity of new phase decreases significantly after the film is polarized to −3 V (blue color bin). To further characterize the effects of Li+ diffusion on the phase change of TiO_2 thin film anode, phase mapping of single layer TiO_2 film under the same cyclic voltages is also conducted for comparison. It is found that no new phase appears after TiO_2 film is polarized to +3 V, indicating that this new phase (~131°) is most likely corresponding to the product of electrochemical reaction involving Li+ insertion. After the quantitative data analysis, the angles of main phase and the intensities of new phase corresponding to the cyclic voltages

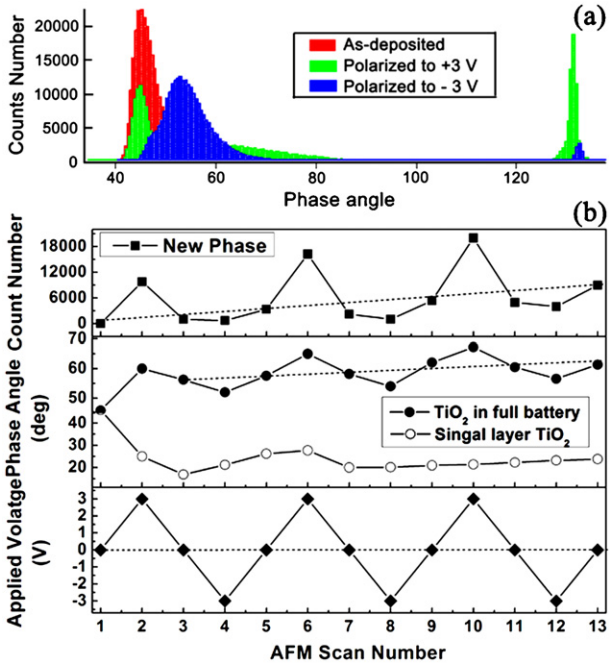

Fig. 4. (a) Distribution histogram of phase angles during the first cycle; (b) analysis of in situ phase images: evolution of main phase angle and new phase intensity *vs.* SPM scan number.

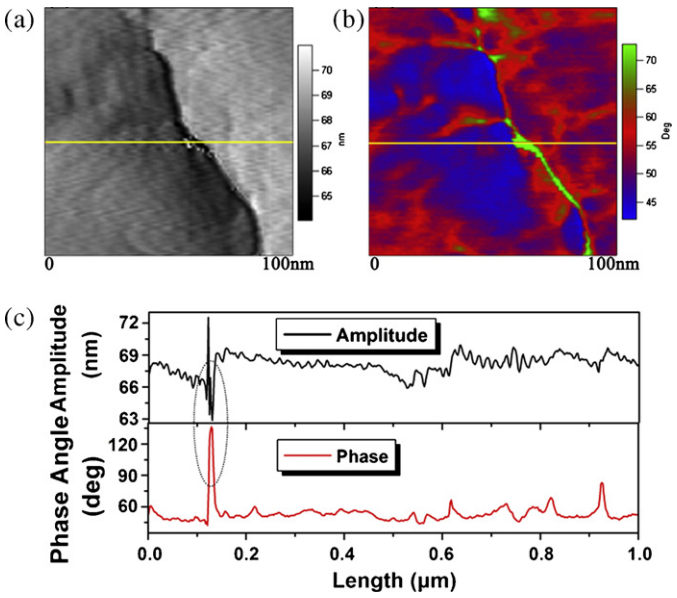

Fig. 5. (a) Magnification of "nano-spots" in amplitude image, and (b) phase image; (c) corresponding line sections of amplitude and corresponding phase images at the same location.

are shown in Fig. 4(b). The trends for both main phase angle and new phase intensity are similar. For single TiO_2 film (Fig. 4(b)), the trend is different from that of TiO_2 thin film anode within the Li-ion battery; the phase angle only decreases during the first cycle and remains nearly unchanged in the subsequent cycles. Considering lithiation/delithiation processes induced by the reversible electrical fields, the cyclic appearance of the new phase should be related to the phase transitions from TiO_2 to Li_xTiO_2 and back to TiO_2 during the lithiation/delithiation cycles. Due to the intrinsic complexity of the phase imaging, the precise and theoretical explanation for the relationship between phase angle shift and Li+ diffusion is still difficult to clarify; however, a possible answer is originated from the change of physical properties of the TiO_2 anode surface due to Li+ insertion/extraction. It is noted that the phase angle shift is mainly originated from the difference in mechanical properties, such as surface hardness, elastic modulus, friction, and adhesion energy [30]. Therefore, compared to the polycrystalline TiO_2 phase, the new phase formed upon Li+ insertion has larger phase angle (~131°), suggesting that the phase has higher surface stiffness and larger adhesion force. Moreover, it is found that the bias-induced phase transition is not fully reversible. The main phase angle increases from ~45° to ~58° after the first cycle, then further increases to ~62° after three cycles. One possible reason is that the local bias-induced phase transformation influences the composition and surface properties of the thin film anode, in addition, the charge trapping/detrapping under different potential states also induces the phase angle shifts.

Combining the phase images and the corresponding deflection images in Fig. 2, some remarkable phenomena can be found. The new phase regions (green) appeared in the phase images corresponds to the "nano-spot" regions in the deflection images [middle column in Fig. 2(b) and (d)], most of those "nano-spots" regions also appear/disappear reversibly under the cyclic electric field. However, when the battery is polarized to −3 V to extract Li+ out of the film, there is still small amount of new phase remaining [green regions in Fig. 2(c) and (e)], indicating that some Li+ are trapped into the thin film anode irreversibly upon Li+ extraction. This is clearly observable in Fig. 5 where the magnification of "nano-spots" and corresponding section lines in both phase and deflection images are presented. The section line profile in the phase image shows a similar track to that in the amplitude image; small phase peaks can be observed at grain boundaries, corresponding to the red lines in the phase images. The new phase (~131°) appears at the length of ~0.13 μm where a peak is also found in the amplitude section line, suggesting that the new phase region has a similar high value of amplitude where the strain is high. The height and area of the "nano-spot" are found to be approximately 1–3 nm and ~1 nm^2, respectively. While the exact explanations for these "nano-spots" are not immediately clear, they should be related to the local movement of Li+ to a great extent. Combining phase and deflection images, it is also found that the "nano-spot" regions are not homogeneously distributed around the anode surface, indicating different amounts of Li+ concentrated by the electrical field. Previous study has suggested that Li+ diffusion through anode is non-uniform including preferred and hindered Li+ diffusion channels [10]. Therefore, the presence of "nano-spots" around the anode surface may provide information on the distribution of Li+ diffusion paths at nanoscale if more evidences can be obtained in future studies. Furthermore, as shown in Fig. 2(e), the distribution of "nano-spots" upon Li+ extraction suggests that most irreversible Li+ is trapped within the grain boundary regions. Hence, grain boundaries play significant roles in the reversible Li+ diffusion during the charge/discharge: first, the electrical field concentrations along grain boundaries are different from the areas within grains; second, the ionic mobility, charge and electron trapping are dissimilar within grain boundaries; third, the irreversible trapping of Li+ upon discharging concentrates within the grain boundaries. Therefore, the control of the grain sizes in the anode at the micro- and nano-scales is very critical in both design and fabrication of Li-ion batteries.

3.3. Cyclic volume changes

Fig. 6(a) shows topography images (height mode) during the Li+ insertion/extraction cycles, where the center 1 μm × 1 μm squares in black frames are dc-writing regions. Scans 2 and 6 are measured as the battery is polarized to 3 V, while scans 4 and 8 are measured as the battery is fully polarized to −3 V. All of the line profiles are measured at the exactly same location on the TiO_2 anode, indicated by the red lines in Fig. 6(a). These line profiles, which are in the direction of perpendicular to the particle gaps, clearly show the nanoscale changes in the relative depth between the two particles. Therefore, the changes of the volume in anode are more straightforward and understandable. As a result, there is no distinct difference between the two scanning images subjecting to the positive bias (scans 2 and 6); one gap between the particles appears in the center (~1.5 μm in length scale). On the other hand, the line profiles after the negative polarization (scans 4 and 8) are also nearly the same. However, compared to the line profiles after the positive polarization, one new particle gap appears at the position of ~1.8 μm in the length scale marked by the red arrow in Fig. 6(a) (scans 4 and 8), indicating the contraction of the thin film anode upon Li+ extraction induced by the negative polarization. It is suggested that the Li+ extraction process (applying −3 V) can create and deepen the gaps between the particles, and Li+ insertion process (applying +3 V) can fill up these gaps reversibly. Furthermore, the volume change of the thin film anode within the battery can be obtained by quantitatively analyzing the line section profiles from the in situ experiments. Surface roughness, a typical parameter to quantify the surface topography, is directly measured using the roughness-analysis tool in the SPM software and represented by the root-mean-squared roughness (RMS). To determine the volume changes of the thin film anode, it is necessary to calculate the changes of the height and area in the fixed region. It is also important that the selected area should be the same for all of the image analysis. However, due to the complex surface structure of thin film

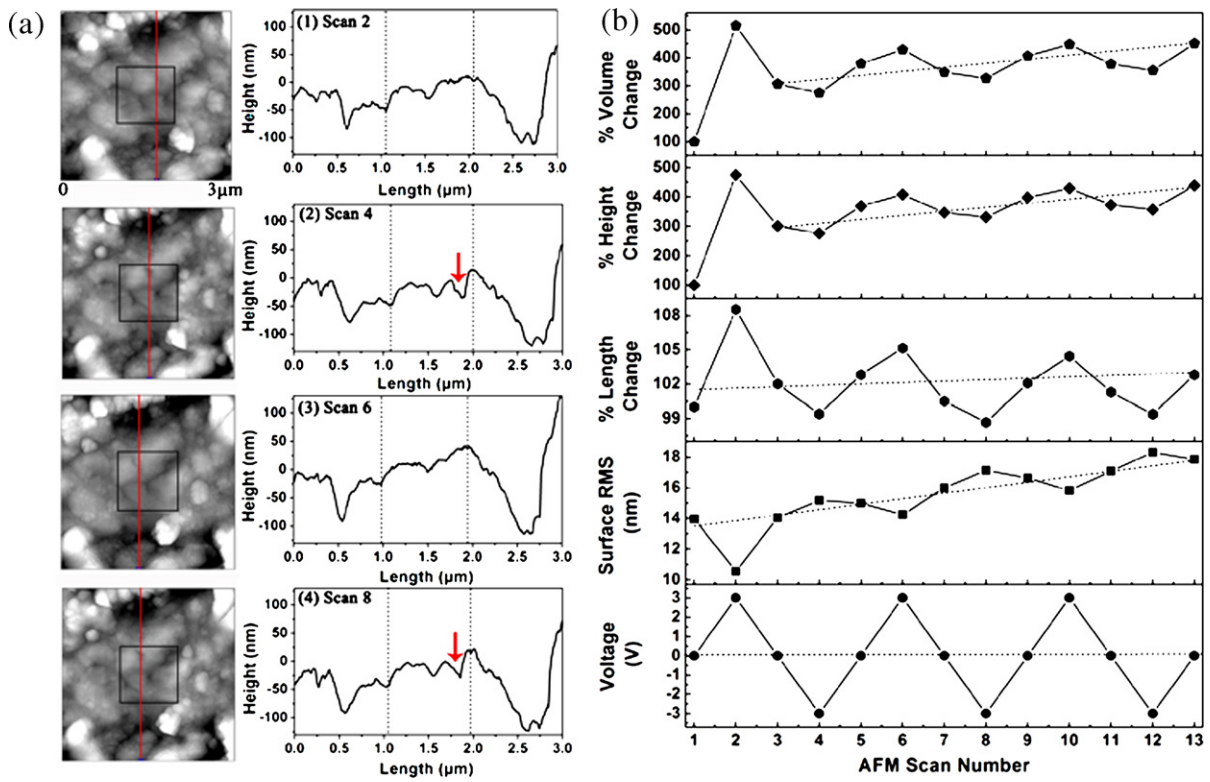

Fig. 6. (a) SPM images (3 μm × 3 μm) and line sections of thin film anode in the selected thin film Li-ion microbattery at the same location, polarized to cyclic potential; (b) analysis of in situ SPM experimental results: percentage changes in surface roughness (RMS), length, height, and volume *vs.* SPM scan number.

anode, it is not possible to get a reliable and accurate measurement of the area of the fixed region. Therefore, in this study, the volume of thin film anode is calculated from the measured height and length of the film along the section line, as the width of line is approximately assumed as unit length. To measure the height changes exactly, height positions of the points in the non-polarized area (outside 1 μm × 1 μm) are used as reference coordinates. Therefore, each line section can be fitted to the same plane in the vertical axis. The average height is obtained by calculating the distance from each point in the line to the reference plane. In the similar way, the average length of the line is calculated by finding two intersections between the line and the reference dotted lines [Fig. 6(a)].

Fig. 6(b) shows the evolution of surface roughness, average length, height and volume of the thin film anode under the cyclic applied voltages. The voltage *vs.* SPM scan number curve in the bottom is described as a series of three insertion/extraction cycles. During the first cycle, surface roughness (RMS) values measured in the polarized area (1 μm × 1 μm squares in black frames) decrease from 13.97 nm to 10.55 nm after the thin film anode is polarized to +3 V (scan 2), and then increases to 15.18 nm after the film is polarized to −3 V (scan 4). In subsequent cycles, the RMS roughness decreases as the Li+ is inserted into the thin film anode and increases as the Li+ is extracted from the film. This phenomenon agrees well with the observation from the topography images, indicating that the film has become flat since it expands in all directions with the particle gaps being filled and closed after positive polarization. Fig. 6(b) also shows the percentage changes in the length, height and volume of the thin film anode. The thin film anode has average change in length of approximately ∼106% as Li+ is inserted into the film (+3 V) and ∼99% as Li+ is removed from the film (−3 V), indicating small changes in the length direction. There may be two reasons for such observations: firstly, the adhesion between the film and the substrate is sufficient; secondly, the holes and gaps between the particles can accommodate most of film expansion in horizontal direction (both length and width). Moreover, it is also proved that the assumption of the width to be unit length has insignificant effects on the calculation results of volume change. Therefore, TiO_2 thin film anode mainly expands vertically by increasing the height. It is found that the height change is very significant for the thin film anode: almost ∼470% during the first Li+ insertion cycle. After the bias is reversed to −3 V (scan 4), the height change only decreases to approximately ∼270%, indicating that the thin film anode cannot return to its initial volume after the first cycle. In subsequent cycles, the film shows average change in height of approximately ∼110% as Li+ is inserted into the film and about ∼89% as Li+ is extracted from the film (reference to the height of scan 5). As shown in the top two graphs in Fig. 6(b), the trend of volume change is similar to that of height change. Due to the permanent trapping of Li+ into the film, both height and volume of TiO_2 thin film anode show increasing trends during the subsequent cycles although the percentage increases in both height and volume have become smaller and more reversible than those in the first cycle.

4. Conclusion

In summary, using biased SPM technique without external electrochemical attachment, we have observed the reversible changes of the surface topography and phase of polycrystalline TiO_2 anode within all-solid-state thin film Li-ion battery induced by local bias-induced electric field; and also quantitatively determined the cyclic volume changes. In addition, although the chemical identification is not available due to the limitation of the SPM set up in this study, phase images can still provide very useful information on the composition and surface property changes during the electrochemical reactions. Therefore, combining simultaneously measurements of phase and amplitude images, high spatially resolved mapping

of "nano-spots" is obtained. These "nano-spots" are most likely related to Li+ distribution in the thin film anode. The measurement of "nano-spots" even shows the spatial resolution below 10 nm. Therefore, this in situ observation related to the Li+ diffusion and trapping at nanoscale provides a new insight into the mechanisms of the ionic transport and the distribution of diffusion preferred paths in real all-solid-state lithium ion battery. Since the information on Li+ permanent trapping is very significant for optimization of the electrochemical performance in the lithium ion battery, more efforts should be made to verify the relationships between the phase and amplitude images in the future studies.

In this work, the battery area of $1\,\mu m \times 1\,\mu m$ shows cyclic expansion/contraction behavior which is attributed to the reversible movement of Li+. The reversible topographic change is particular within the gaps between grain particles, which are filled up and reopened during the Li+ insertion/extraction processes. This phenomenon is analogous to what observed in the traditional EC-AFM studies, suggesting that the local cyclic voltage can be used for modeling the charge/discharge processes in the lithium ion battery. Therefore, this simple SPM method is very promising for in situ characterization of the electrochemical mechanisms and ionic distribution of lithium ion batteries during Li+ insertion/extraction at nanoscale, especially valuable for all-solid state thin film batteries without liquid, in which the ionic and electron transfer within the solid has not been widely studied before.

Acknowledgements

This work was supported by Agency for Science, Technology and Research (A*STAR), Singapore under research project 0721340051 (R-265-000-292-305) and the Ministry of Education, Singapore through National University of Singapore under Academic Research Funds (R265-000-305-112).

References

[1] J.J. Ding, Q.A. Sun, Z.W. Fu, Electrochem. Solid State Lett. 13 (2010) A105–A108.
[2] A. Patil, V. Patil, D. Wook Shin, J.-W. Choi, D.-S. Paik, S.-J. Yoon, Mater. Res. Bull. 43 (2008) 1913–1942.
[3] J.L. Souquet, M. Duclot, Solid State Ionics 148 (2002) 375–379.
[4] S.V. Kalinin, N. Balke, Adv. Mater. 22 (2010) E193–E209.
[5] G. Benstetter, R. Biberger, D. Liu, Thin Solid Films 517 (2009) 5100–5105.
[6] M. Jaquith, E.M. Muller, J.A. Marohn, J. Phys. Chem. B 111 (2007) 7711–7714.
[7] S.V. Kalinin, B.J. Rodriguez, S. Jesse, P. Maksymovych, K. Seal, M. Nikiforov, A.P. Baddorf, A.L. Kholkin, R. Proksch, Mater. Today 11 (2008) 16–27.
[8] L. Zhang, T. Sakai, N. Sakuma, T. Ono, K. Nakayama, Appl. Phys. Lett. 75 (1999) 3527–3529.
[9] N. Balke, S. Jesse, Y. Kim, L. Adamczyk, I.N. Ivanov, N.J. Dudney, S.V. Kalinin, ACS Nano 4 (2010) 7349–7357.
[10] N. Balke, S. Jesse, Y. Kim, L. Adamczyk, A. Tselev, I.N. Ivanov, N.J. Dudney, S.V. Kalinin, Nano Lett. 10 (2010) 3420–3425.
[11] N. Balke, S. Jesse, A.N. Morozovska, E. Eliseev, D.W. Chung, Y. Kim, L. Adamczyk, R.E. Garcia, N.J. Dudney, S.V. Kalinin, Nat. Nano 5 (2010) 749–754.
[12] L.Y. Beaulieu, S.D. Beattie, T.D. Hatchard, J.R. Dahn, J. Electrochem. Soc. 150 (2003) A419–A424.
[13] L.Y. Beaulieu, T.D. Hatchard, A. Bonakdarpour, M.D. Fleischauer, J.R. Dahn, J. Electrochem. Soc. 150 (2003) A1457–A1464.
[14] A. Clemencon, A.T. Appapillai, S. Kumar, Y. Shao-Horn, Electrochim. Acta 52 (2007) 4572–4580.
[15] M. Koltypin, Y.S. Cohen, B. Markovsky, Y. Cohen, D. Aurbach, Electrochem. Commun. 4 (2002) 17–23.
[16] K. Kushida, K. Kuriyama, Appl. Phys. Lett. 84 (2004) 3456–3458.
[17] A.N. Morozovska, E.A. Eliseev, N. Balke, S.V. Kalinin, J. Appl. Phys. 108 (2010) 053712.
[18] A.N. Morozovska, E.A. Eliseev, S.V. Kalinin, Appl. Phys. Lett. 96 (2010) 222906.
[19] J. Swiatowska-Mrowiecka, V. Maurice, L. Klein, P. Marcus, Electrochem. Commun. 9 (2007) 2448–2455.
[20] L.Y. Beaulieu, A.D. Rutenberg, J.R. Dahn, Microsc. Microanal. 8 (2002) 422–428.
[21] T. Doi, M. Inaba, H. Tsuchiya, S.-K. Jeong, Y. Iriyama, T. Abe, Z. Ogumi, J. Power Sources 180 (2008) 539–545.
[22] F. Kong, R. Kostecki, G. Nadeau, X. Song, K. Zaghib, K. Kinoshita, F. McLarnon, J. Power Sources 97–98 (2001) 58–66.
[23] K. Kuriyama, A. Onoue, Y. Yuasa, K. Kushida, Surf. Sci. 601 (2007) 2256–2259.
[24] P.R. Singh, S. Mahajan, S. Rajwade, A.Q. Contractor, J. Electroanal. Chem. 625 (2009) 16–26.
[25] J. Swiatowska-Mrowiecka, V. Maurice, S. Zanna, L. Klein, E. Briand, I. Vickridge, P. Marcus, J. Power Sources 170 (2007) 160–172.
[26] J. Vetter, P. Novak, M.R. Wagner, C. Veit, K.C. M¨oller, J.O. Besenhard, M. Winter, M. WohlfahrtMehrens, C. Vogler, A. Hammouche, J. Power Sources 147 (2005) 269–281.
[27] J.B. Bates, N.J. Dudney, B. Neudecker, A. Ueda, C.D. Evans, Solid State Ionics 135 (2000) 33–45.
[28] S.N. Magonov, V. Elings, M.H. Whangbo, Surf. Sci. 375 (1997) L385–L391.
[29] P. Schon, K. Bagdi, K. Molnar, P. Markus, B. Pukanszky, G.J. Vancso, Eur. Polym. J. 47 (2011) 692–698.
[30] S. Thanawan, S. Radabutra, P. Thamasirianunt, T. Amornsakchai, K. Suchiva, Ultramicroscopy 109 (2009) 189–192.